Thermal Quench Dynamics and Heat Flux Distribution during Massive-Impurity-Injection Triggered Disruption in EAST

L. Zeng, W. Xia, D. Hu, Y. Sun, T. Tang, X. Zhu, S. Zhao, T. Shi, D. Chen, Y. Duan, L. Xu, G. Li, G. Zuo, J. Hu, X. Gao, Z. Gao, the JOREK Team*

Department of Engineering Physics, Tsinghua University
Institute of Plasma Physics, Chinese Academy of Sciences, Hefei, China
University of Science and Technology of China, Hefei, China
School of Physics, Beihang University, Beijing, China
Advanced Energy Research Center, Shenzhen University, Shenzhen, China
***See Hoelzl *et al* 2024 (https://doi.org/10.1088/1741-4326/ad5a21) for the JOREK Team**

Thermal quench poses serious threat to PFCs

- **Thermal quench (TQ) process can cause unacceptable heat load on PFCs in ITER.**
  - The stored thermal energy at TQ
  - The duration of TQ and deposition area on PFCs

Massive impurity injection could decrease the PFC energy deposition

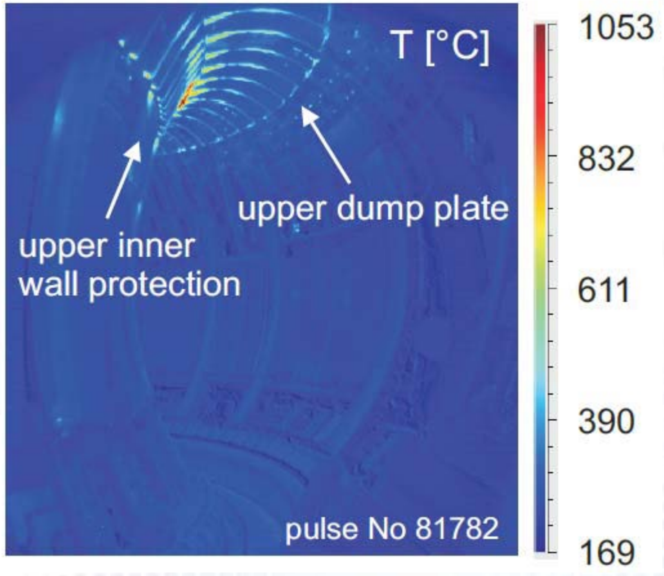

J. Nucl. Mater. 438 (2013) S102-S107

Thermal quench poses serious threat to PFCs

- **Thermal quench (TQ) process can cause unacceptable heat load on PFCs in ITER.**
  - The stored thermal energy at TQ
  - The duration of TQ and deposition area on PFCs

Massive impurity injection could decrease the PFC energy deposition

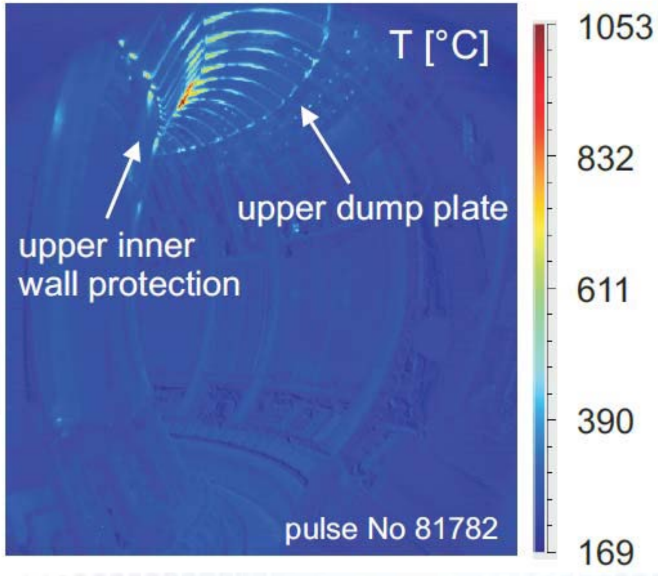

- **Talk presents results for:**
  - Impurity transport during massive-impurity-injection triggered disruptions
  - TQ process on EAST and its interpretive MHD modelling with JOREK

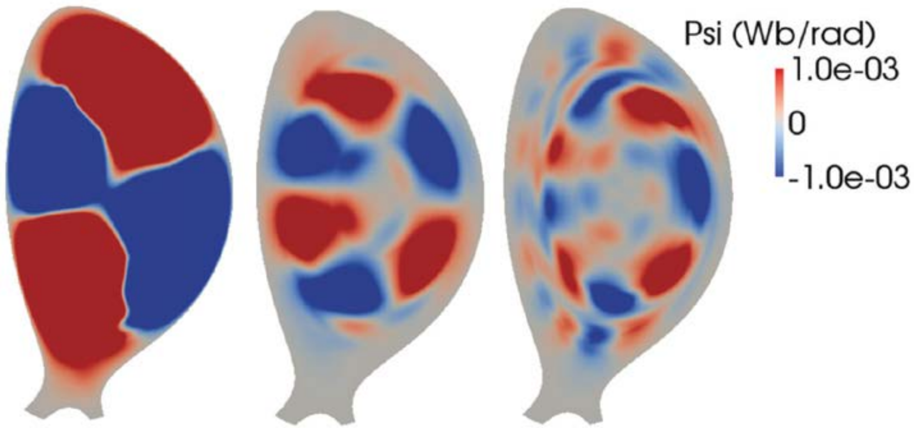

J. Nucl. Mater. 438 (2013) S102-S107
EPS (2018) P4.1043

Characteristics of disruption mitigation via SPI and MGI

- Both **shattered pellet injection (SPI) and massive gas injection (MGI)** technologies have been developed for disruption mitigation on EAST.
  - **SPI**: ***Ne, H_2+Ne***; ***Pellet speed < 400 m/s.***
  - **MGI**: ***Ar, Ne, He, D_2***; ***Response time < 1 ms.***

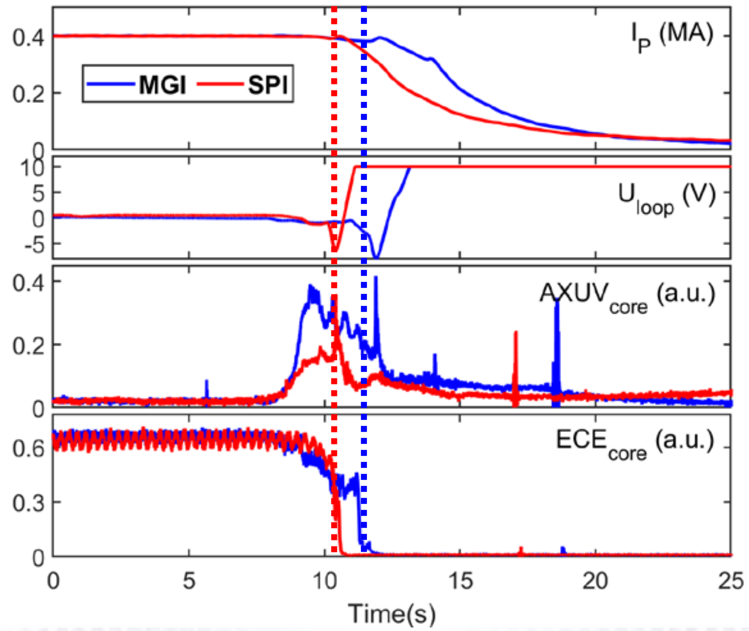

Rev. Sci. Instrum. 86 (2015) 053502;
Fusion Eng. Des. 191 (2023) 113567;Nucl. Fusion 65 (2025) 016048

Characteristics of disruption mitigation via SPI and MGI

- **Both shattered pellet injection (SPI) and massive gas injection (MGI) technologies have been developed for disruption mitigation on EAST.**
  - **SPI**: ***Ne, H_2+Ne; Pellet speed < 400 m/s.***
  - **MGI**: ***Ar, Ne, He, D_2; Response time < 1 ms.***

- **Intended disruption triggered by SPI and MGI**
  - ***While MGI tends to deposit more impurities at the edge, SPI penetrates deeper into the plasma and results in a shorter overall disruption duration.***
  - ***The impurity trajectory is highly asymmetric in both the toroidal and poloidal directions.***

No clear difference in TQ process found

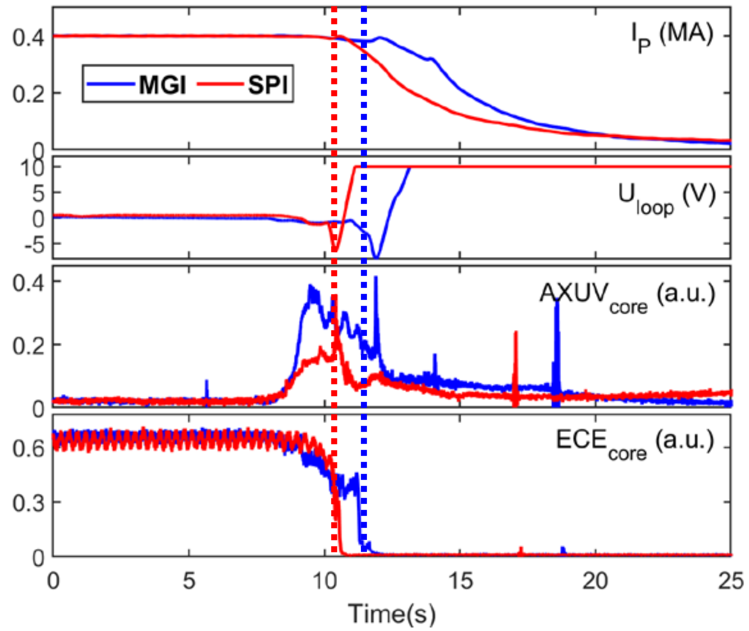

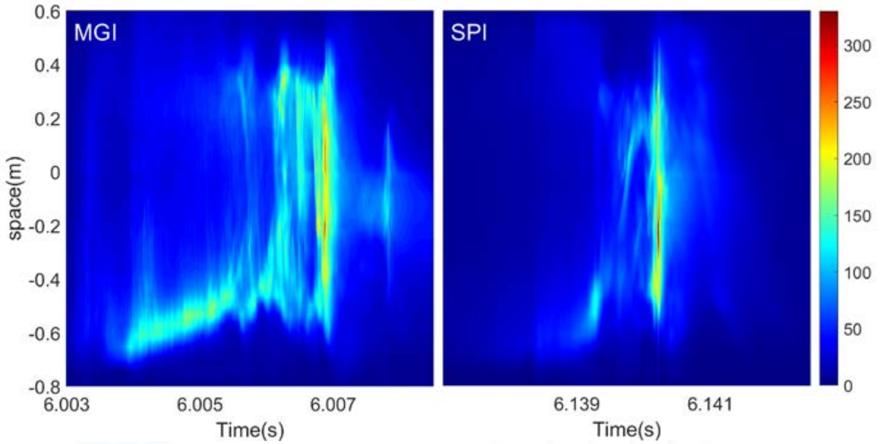

Rev. Sci. Instrum. 86 (2015) 053502;
Fusion Eng. Des. 191 (2023) 113567;Nucl. Fusion 65 (2025) 016048

Typical TQ process in the EAST disruptions

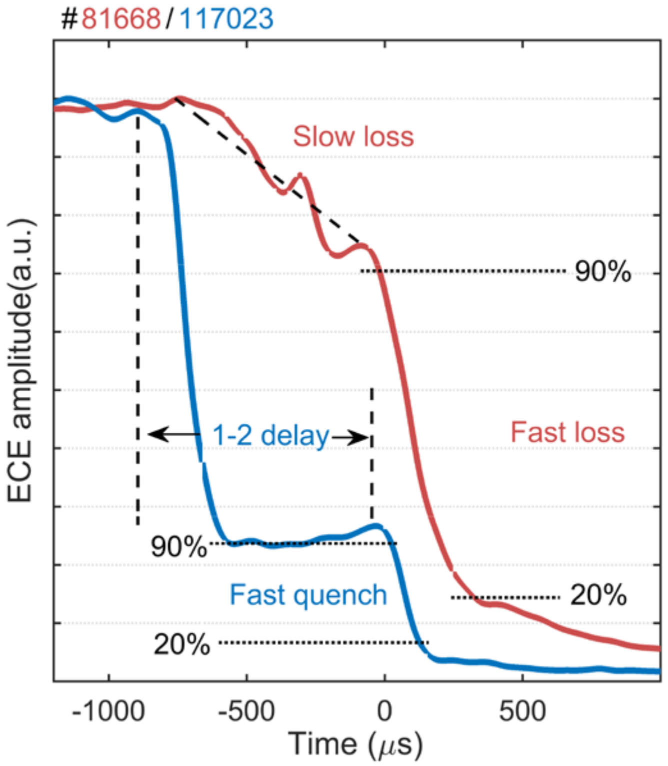

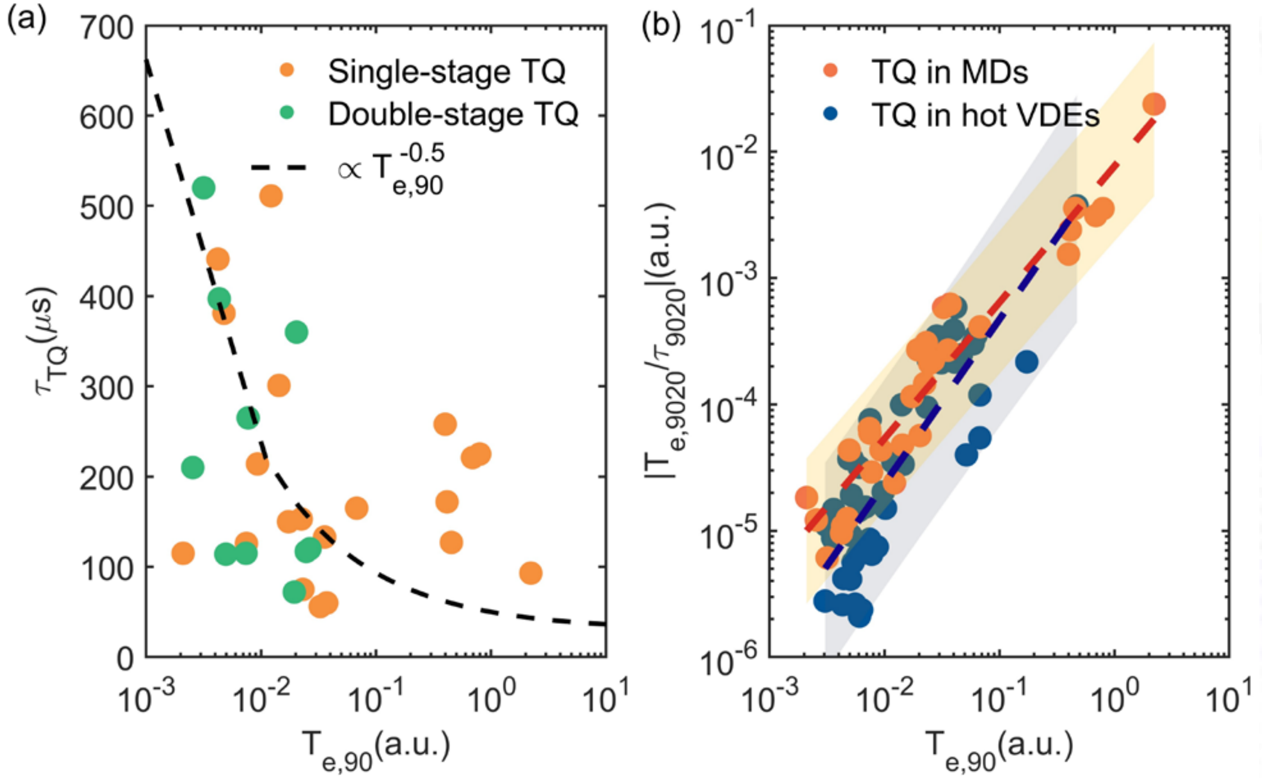

- **Single-stage TQ and double-stage TQ during disruptions.**
- **A large range at the low temperature and short TQ durations at high T_e, not fully consistent with $T_e^{-0.5}$.**

***TQ duration: The time intervals between 90%-20%**

Plasma Phys. Control. Fusion 65 (2023) 085011

Impurity transport during the pre-TQ phase

Rotation direction of magnetic island observed to reverse in the pre-TQ phase

- **The 2/1 mode's rotation slows down and then reverses from the ion diamagnetic to the electron diamagnetic direction after neon injection into co-current NBI-heating plasmas.**
  - *The mode frequency changes from 2 kHz to −3 kHz in < 0.5 ms.*

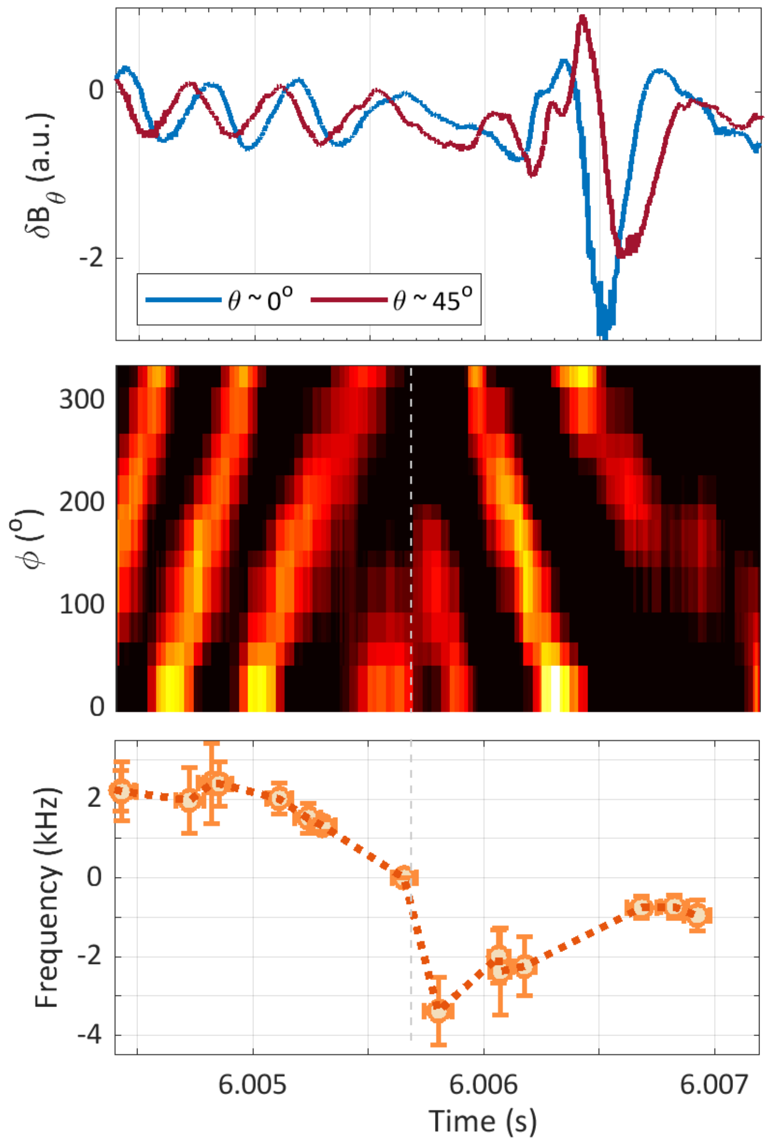

Nucl. Fusion 65 (2025) 016048

Rotation direction of magnetic island observed to reverse in the pre-TQ phase

- The 2/1 mode's rotation slows down and then **reverses from the ion diamagnetic to the electron diamagnetic direction** after neon injection into co-current NBI-heating plasmas.
  - *The mode frequency changes from 2 kHz to −3 kHz in < 0.5 ms.*

- **The radiation in the core region significantly increases** following the rotation direction of the mode reversed.

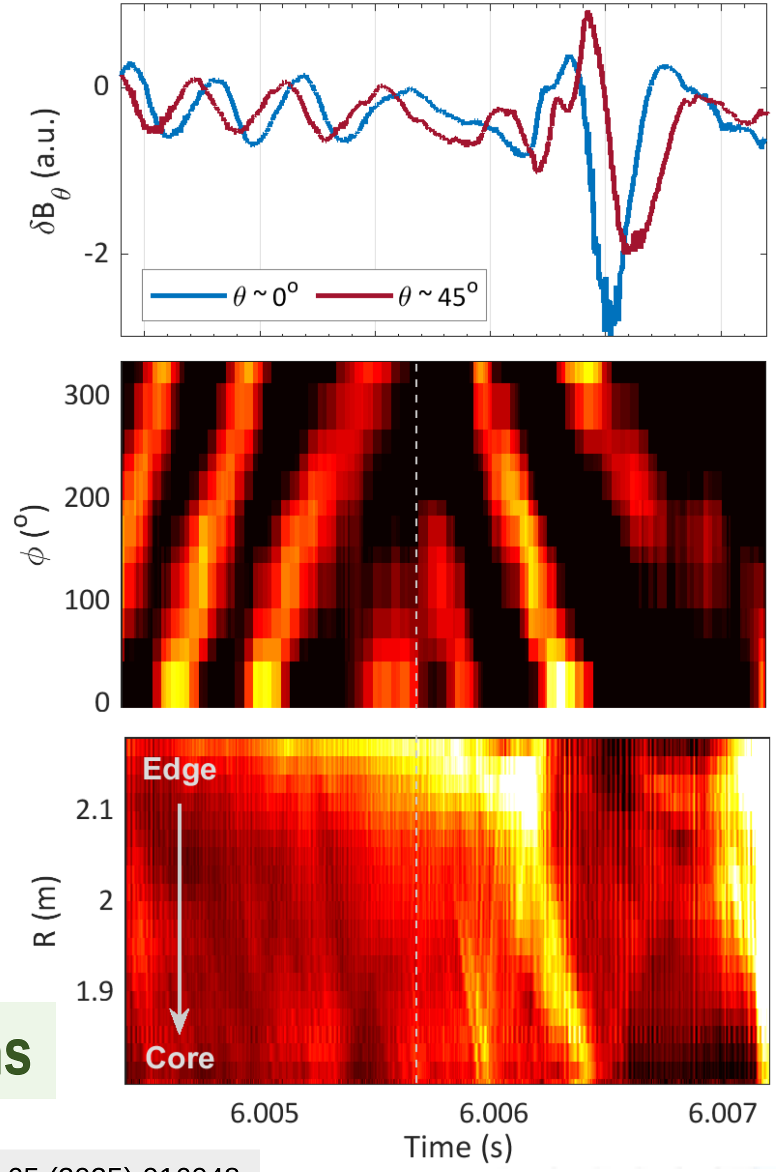

Observed in both SPI and MGI triggered disruptions

Nucl. Fusion 65 (2025) 016048

The core radiation enhanced following the rotation direction of the mode reversed

- **The impurity influx divided into two stages according to the XUV and SXR detectors.**
  - ***STAGE 1**: impurities drift along ion diamagnetic direction; Outside of q=2 surface. Inward pinch speed ~ 60 m/s.*

Rotation direction of the mode reversed

  - ***STAGE 2**: impurities drift along electron diamagnetic direction; Across q=2 surface. Inward pinch speed ~ 300 m/s.*

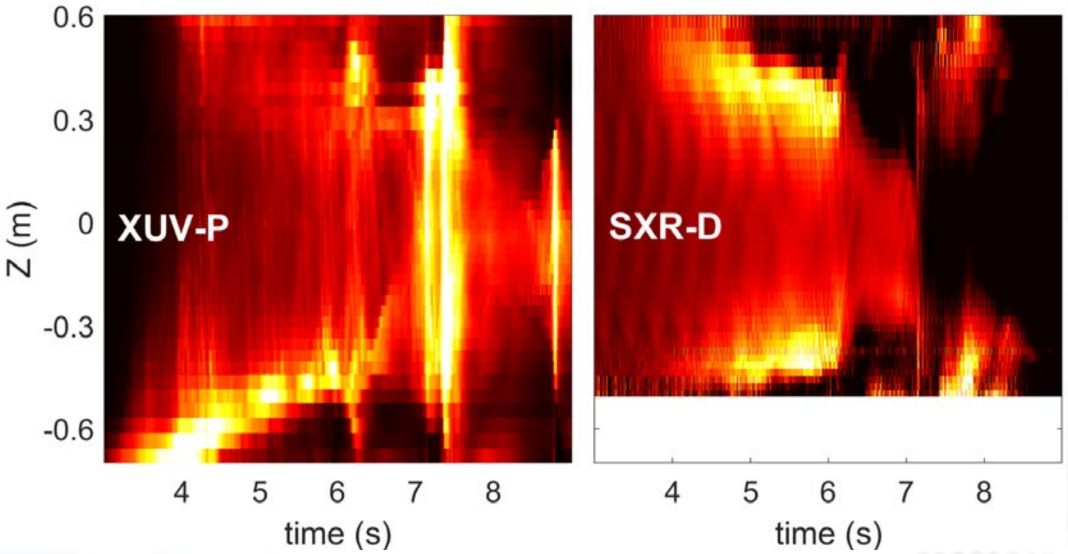

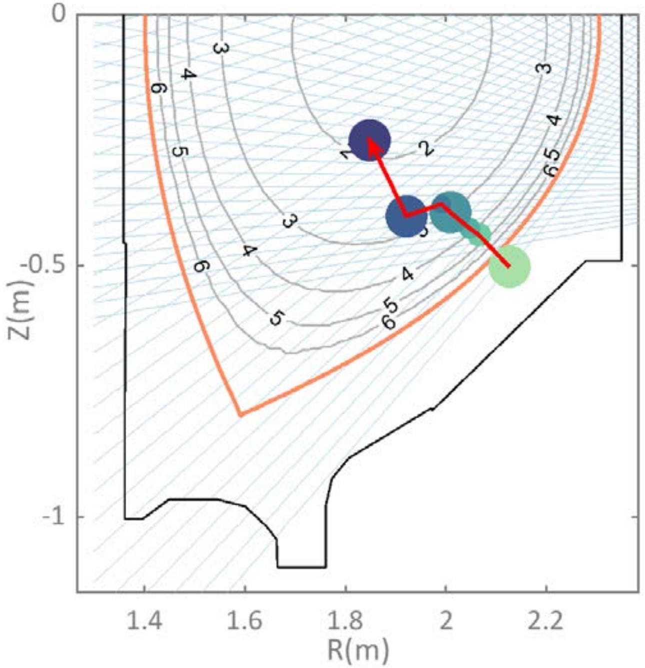

Parameter dependence of mode-frequency change

- **The phenomenon has been observed by scanning species and numbers of impurities, and heating methods.**
  - ***Amount scan: Earlier and faster reversion of rotation direction.***

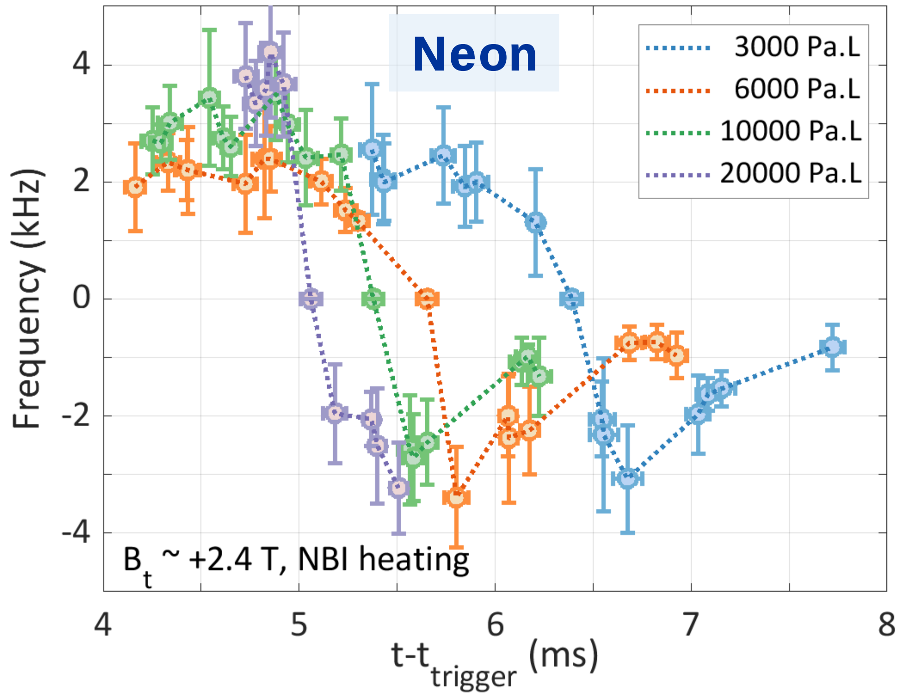

Parameter dependence of mode-frequency change

- **The phenomenon has been observed by scanning species and numbers of impurities, and heating methods.**
  - ***Amount scan: Earlier and faster reversion of rotation direction.***
  - ***The mode frequency changes from −5 kHz to −9 kHz in ~ 0.5 ms after argon injection into RF-heating plasmas.***
  - ***The mode frequency after argon injection seems lower than after neon injection.***

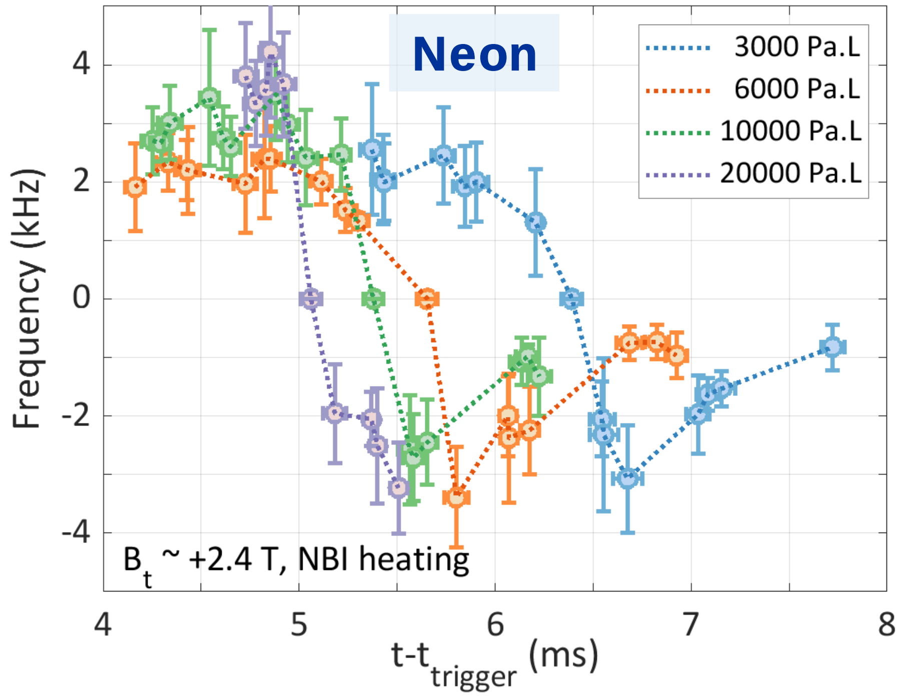

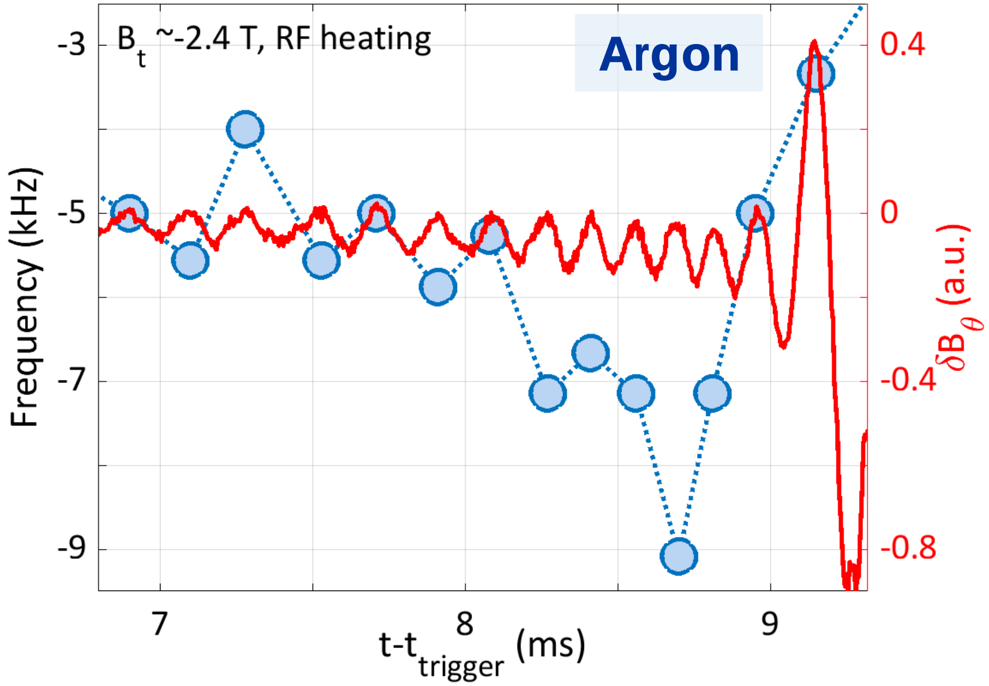

Change of mode frequency is mainly caused by poloidal angular frequency

- **Frequency of (2,1) tearing mode is written as**

$$2\pi \cdot f_{\mathrm{MHD}} = \Omega_{\boldsymbol{E}\times\boldsymbol{B}} + \Omega_{*e} + 0.71\Omega_{*T_e}$$

  - $\Omega_{E\times B}$ ***can be determined by ion radial force balance equation.***

$$\Omega_{\boldsymbol{E}\times\boldsymbol{B}} = \boldsymbol{U} \cdot \nabla\zeta - q\boldsymbol{U} \cdot \nabla\theta - \Omega_{*i}$$

Change of mode frequency is mainly caused by poloidal angular frequency

- **Frequency of (2,1) tearing mode is written as**

$$2\pi \cdot f_{\mathrm{MHD}} = \Omega_{E\times B} + \Omega_{*e} + 0.71\Omega_{*T_e}$$

  - $\Omega_{E\times B}$ ***can be determined by ion radial force balance equation.***

$$\Omega_{E\times B} = \boldsymbol{U}\cdot\nabla\zeta - q\boldsymbol{U}\cdot\nabla\theta - \Omega_{*i}$$

  - **The reversed time scale (< 0.5 ms) is much less than energy confinement time and momentum transport time, so the change of mode frequency is mainly caused by poloidal angular frequency.**

Poloidal rotation velocity

$$\delta U_\theta = -\frac{B_T}{B^2}\delta E_r$$

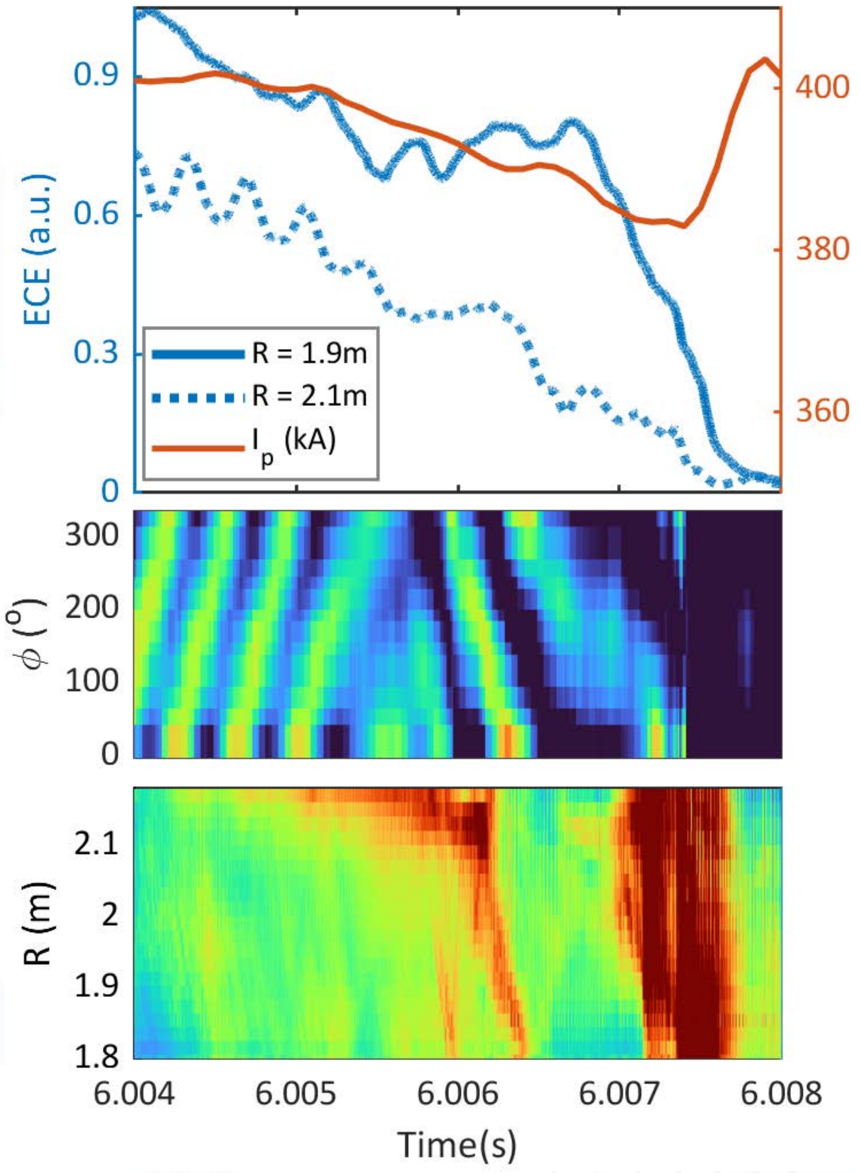

The neoclassical theory is applied to understand the phenomenon

- **Time scale of frequency change (< 0.5 ms) is much less than τ_E (50-100 ms) on EAST.**
  - ***The neoclassical relaxation time in the collisional regime*** **τ_θ < 0.5 ms ($\tau_\theta \simeq q^2 R^2 \nu_i / v_{T_i}^2$).**

The neoclassical theory ☺

The neoclassical theory is applied to understand the phenomenon

- **Time scale of frequency change (< 0.5 ms) is much less than τ_E (50-100 ms) on EAST.**
  - ***The neoclassical relaxation time in the collisional regime τ_θ < 0.5 ms ($\tau_\theta \simeq q^2R^2\nu_i/v_{T_i}^2$).***

The neoclassical theory ☺

- **The poloidal rotation can be driven by the viscosity associated with the collisionality and impurity.**
  - ***In standard neoclassical theory, the poloidal component of the perpendicular E×B drift is damped by the poloidal (parallel) viscosity.***

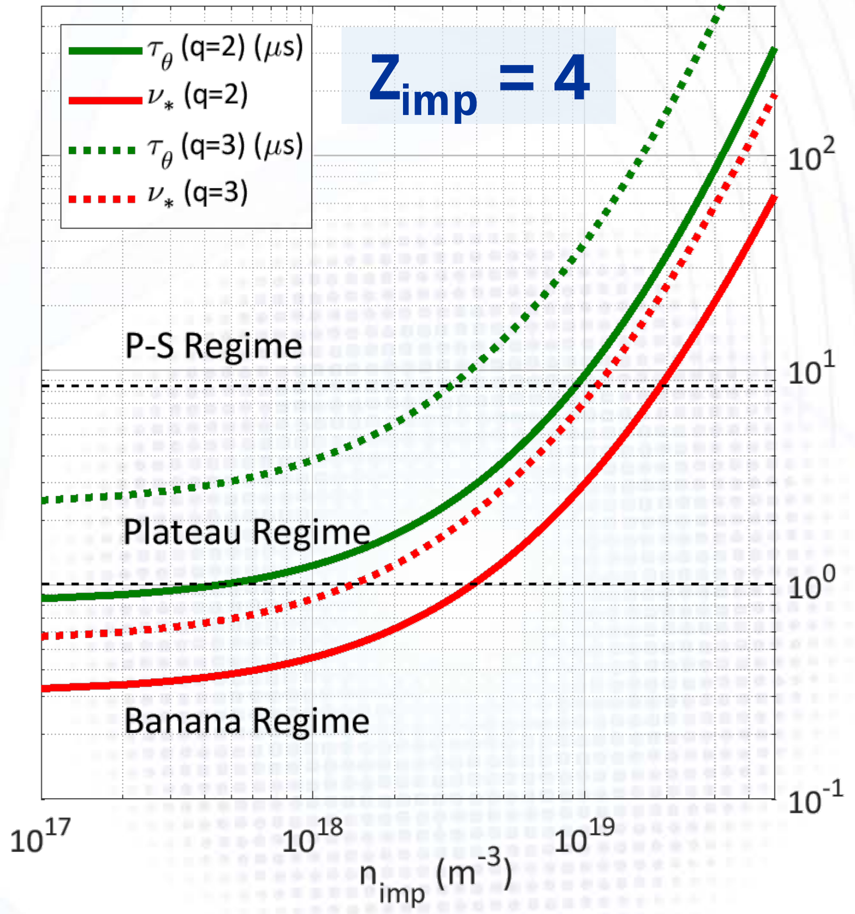

A model for poloidal rotation during the transient state

- **The parallel momentum and heat flow balance equations for the impurity and ion species in the form of matrix equations are as followed.**
  - ***particle and heat flow of impurity, radial electric field, and ion heat flow* included.**

$$
\begin{bmatrix}
\frac{n_I m_I \tau_{ii}}{n_i m_i \tau_{II}}\mu_{00}^I + \alpha & \frac{n_I m_I \tau_{ii}}{n_i m_i \tau_{II}}\mu_{01}^I & \alpha\frac{B_T}{B_p} & -1.5\alpha \\
\frac{n_I m_I \tau_{ii}}{n_i m_i \tau_{II}}\mu_{10}^I & \frac{n_I m_I \tau_{ii}}{n_i m_i \tau_{II}}\mu_{11}^I + \alpha\frac{T_i}{T_I}\left(7.5+\sqrt{2}\alpha x^{-1}\right) & 0 & -6.75\alpha x^2 \\
-\alpha & 0 & -\mu_{00}^i\frac{B_T}{B_p} - \alpha\frac{B_T}{B_p} & \mu_{01}^i + 1.5\alpha \\
-1.5\alpha & -6.75\frac{T_i}{T_I}\alpha x^2 & -\mu_{10}^i\frac{B_T}{B_p} - 1.5\alpha\frac{B_T}{B_p} & \mu_{11}^i + \left(\sqrt{2}+3.25\alpha\right)
\end{bmatrix}
\begin{bmatrix}
u_{0\theta}^I B^2 \\ u_{1\theta}^I B^2 \\ E_r \\ u_{1\theta}^i B^2
\end{bmatrix}
$$

$$
= \begin{bmatrix}
\alpha\frac{B_T T_I}{e_I B_p L_{pI}} + \alpha U_{0\parallel}^i B + 1.5\alpha\frac{B_T T_i}{B_p e_i L_{Ti}} \\
\alpha\frac{T_i}{T_I}\left(7.5+\sqrt{2}\alpha x^{-1}\right)\frac{B_T T_I}{B_p e_I L_{TI}} + 6.75\alpha x^2\frac{B_T T_i}{B_p e_i L_{Ti}} \\
-\mu_{00}^i U_{0\parallel}^i B - \mu_{00}^i\frac{B_T T_i}{e_i B_p L_{pi}} - \alpha U_{0\parallel}^i B - 1.5\alpha\frac{B_T T_i}{B_p e_i L_{Ti}} - \alpha\frac{B_T T_I}{B_p e_I L_{TI}} \\
-\mu_{10}^i U_{0\parallel}^i B - \mu_{10}^i\frac{B_T T_i}{B_p e_i L_{pi}} - 1.5\alpha U_{0\parallel}^i B - \left(\sqrt{2}+3.25\alpha\right)\frac{B_T T_i}{B_p e_i L_{Ti}} - 1.5\alpha\frac{B_T T_I}{e_I B_p L_{pI}} + 6.75\frac{T_i}{T_I}\alpha x^2\frac{B_T T_I}{B_p e_I L_{TI}}
\end{bmatrix}
$$

$\alpha \equiv n_I Z_I^2 / n_i Z_i^2$

(Impurity strength parameter)

$x \equiv V_{th,I}/V_{th,i} \ll 1$

Nucl. Fusion 21 (1981) 1079
Phys. Fluids B 3 (1991) 2050

Effect of collisionality and impurity on radial electric field

- **A clear change in radial electric field is observed as collisionality transitions from the banana to the P–S regime.**
  - ***As the ion collisionality increases, the radial electric field decrease nonlinearly.***

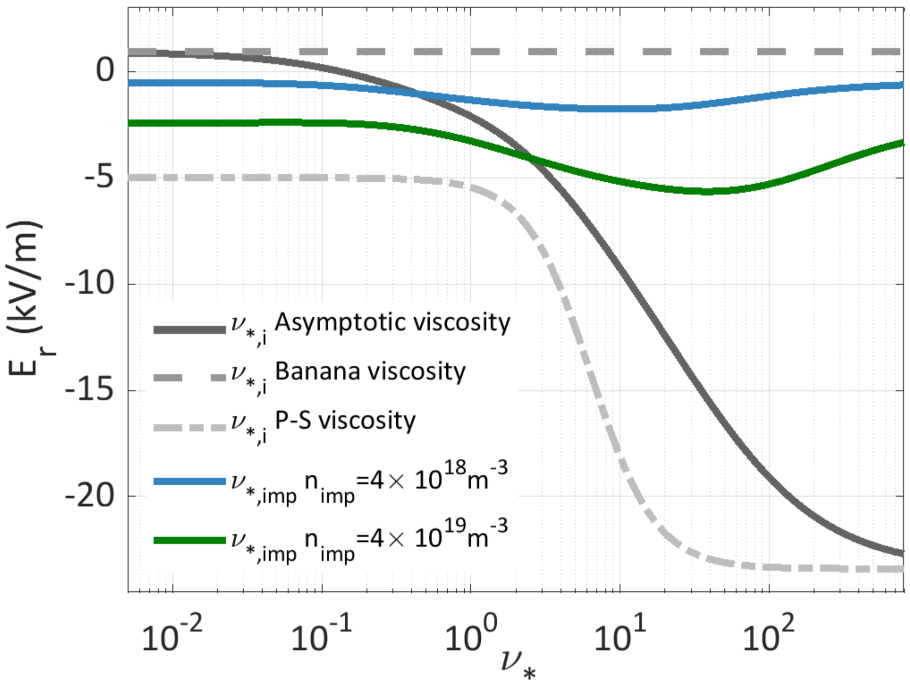

Effect of collisionality and impurity on radial electric field

- **A clear change in radial electric field is observed as collisionality transitions from the banana to the P–S regime.**
  - ***As the ion collisionality increases, the radial electric field decrease nonlinearly.***
  - ***The viscosity is sensitive to impurity strength: impurity orbits perturb ion orbits and thereby alter the effective viscosity.***

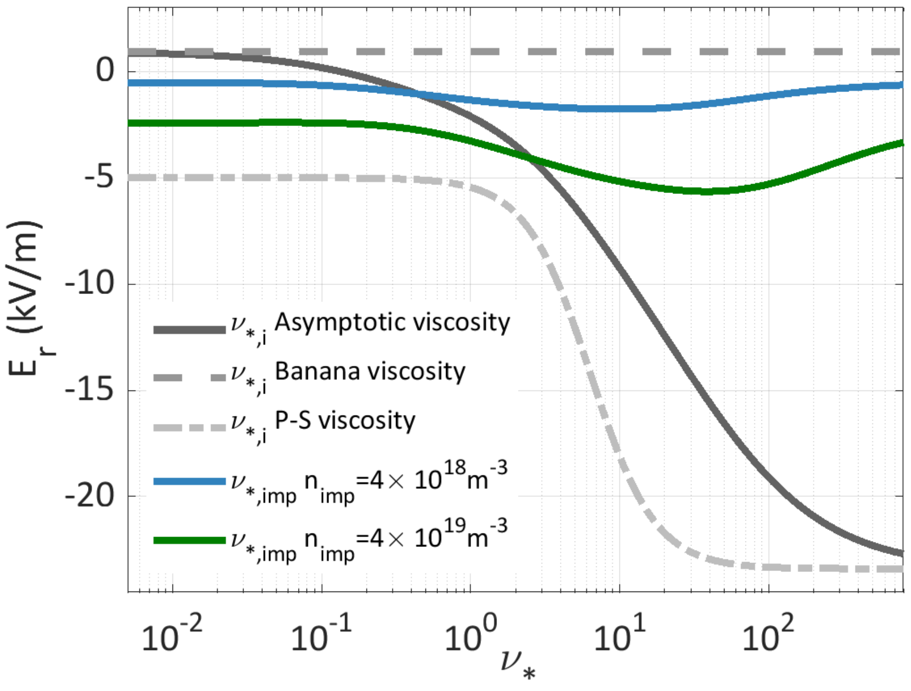

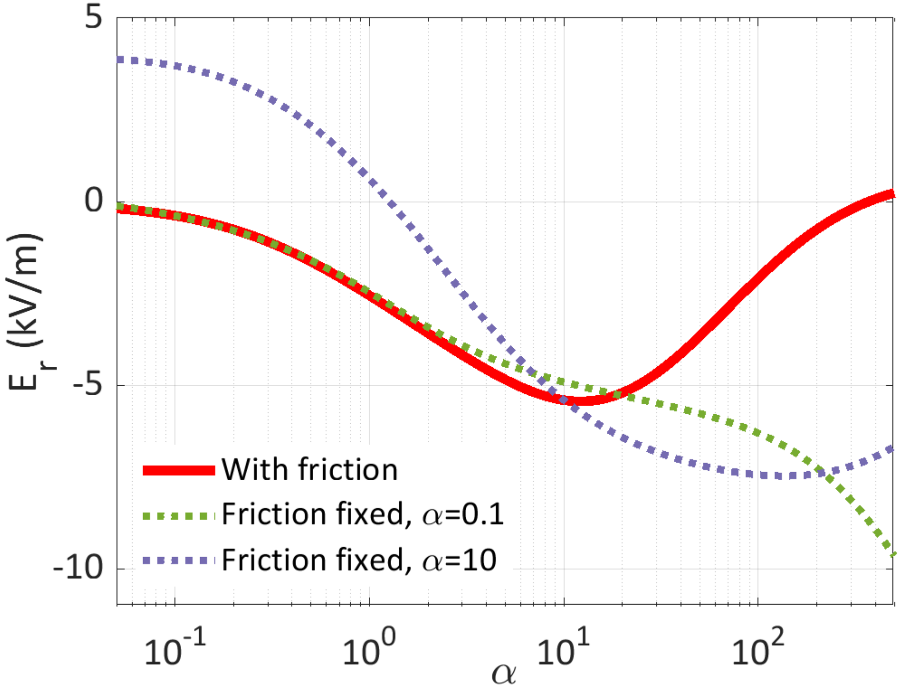

E_r estimated from the model is consistent with the experimental value

- **Global effects with massive impurity injection show that:**
  - ***The ion poloidal velocity is directed toward the ion-diamagnetic side, whereas the impurity poloidal velocity is directed toward the electron-diamagnetic side.***
  - ***Variations in the ion poloidal flow are governed by the E×B drift.***
    - **The magnitude of the radial electric field increases as the ion-temperature gradient steepens.**

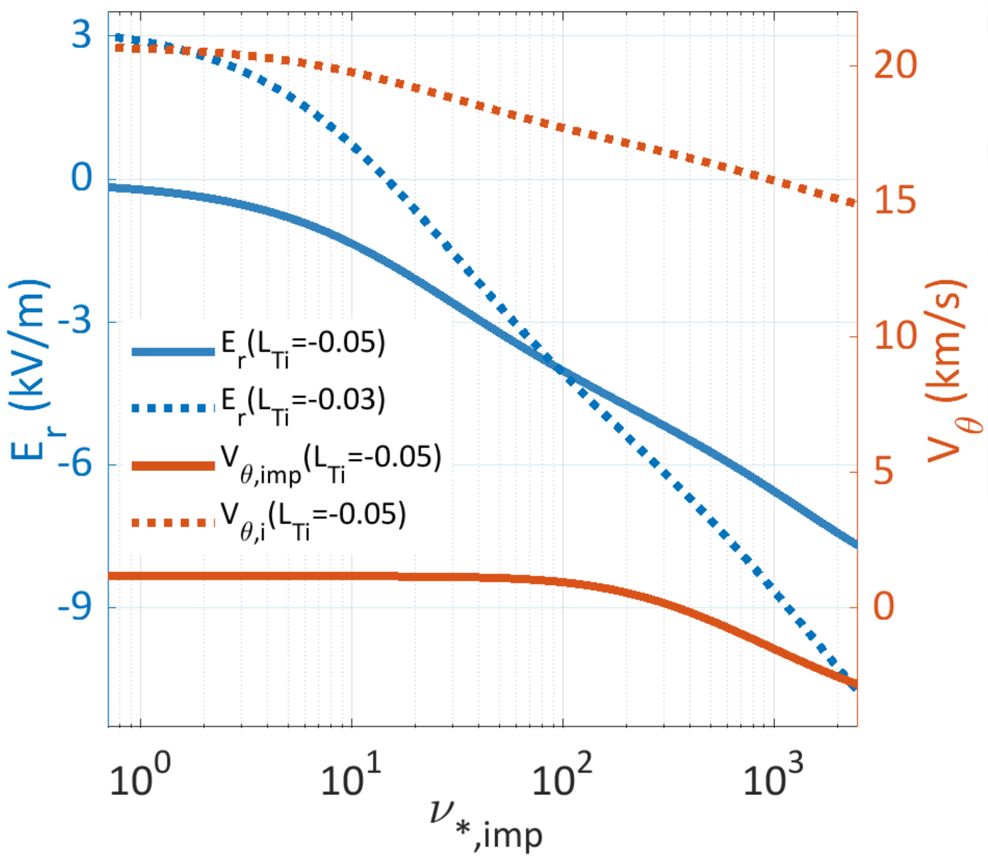

E_r estimated from the model is consistent with the experimental value

- **Global effects with massive impurity injection show that:**
  - ***The ion poloidal velocity is directed toward the ion-diamagnetic side, whereas the impurity poloidal velocity is directed toward the electron-diamagnetic side.***
  - ***Variations in the ion poloidal flow are governed by the E×B drift*.**
    - **The magnitude of the radial electric field increases as the ion-temperature gradient steepens.**

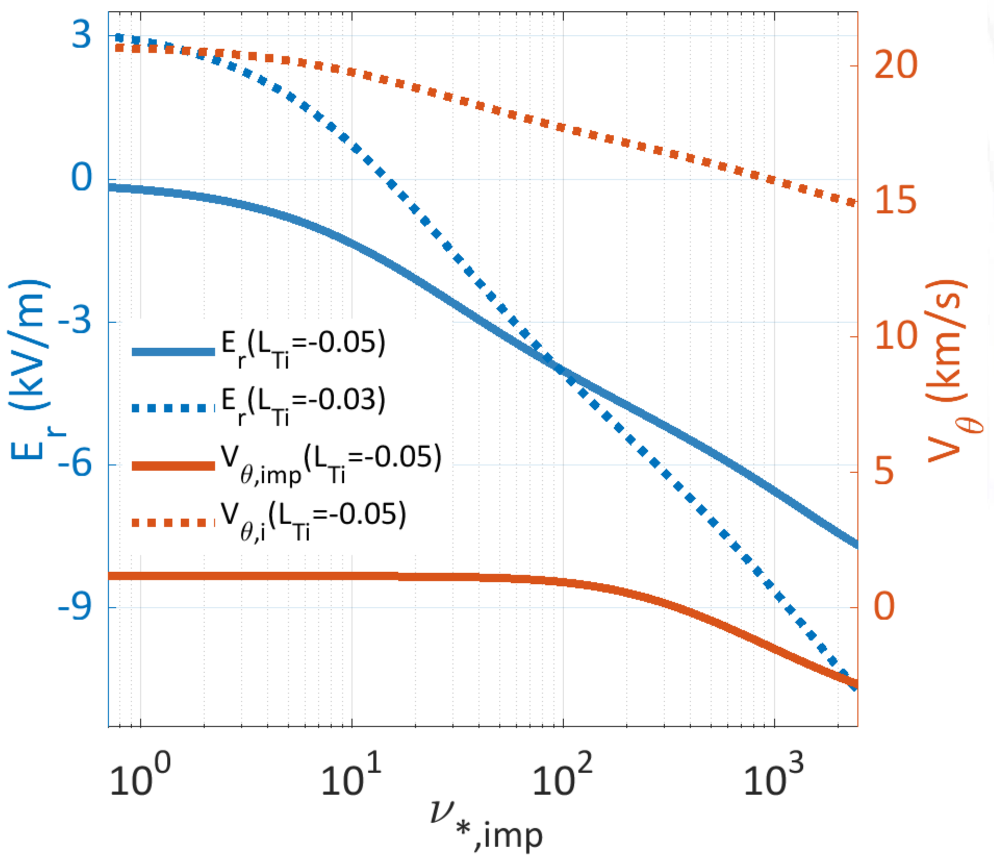

E_r is estimated in the range from −12 kV/m to −8 kV/m according to the typical parameters, consistent with the experimental value of ~ −10 kV/m.

Evolution of plasma parameters presents clear change in collisionality and amount of impurity

- **Simulation results via JOREK with fixed viscosity show that the collisionality increases quickly from the banana to the P-S regime.**

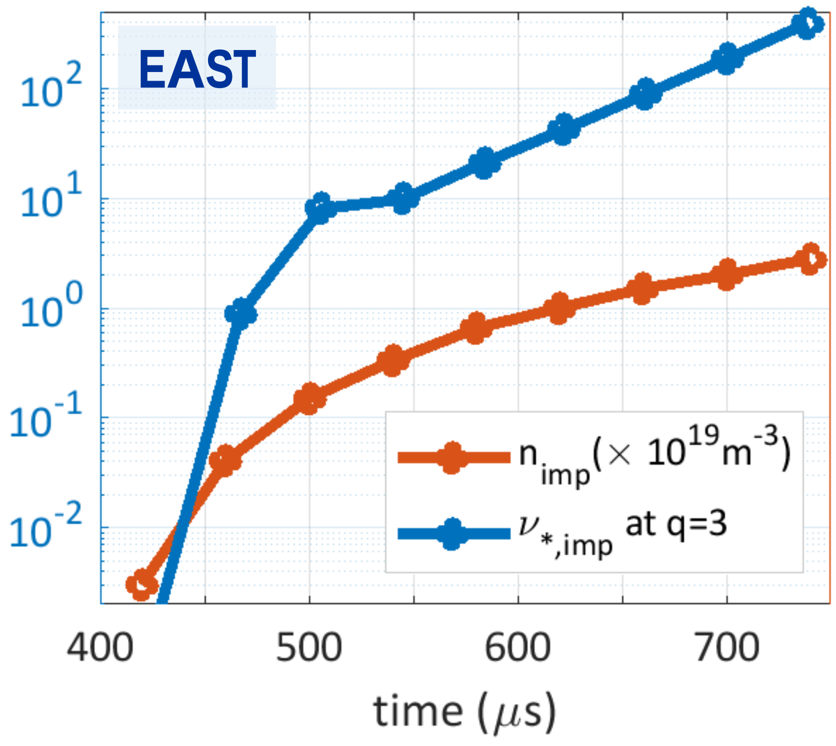

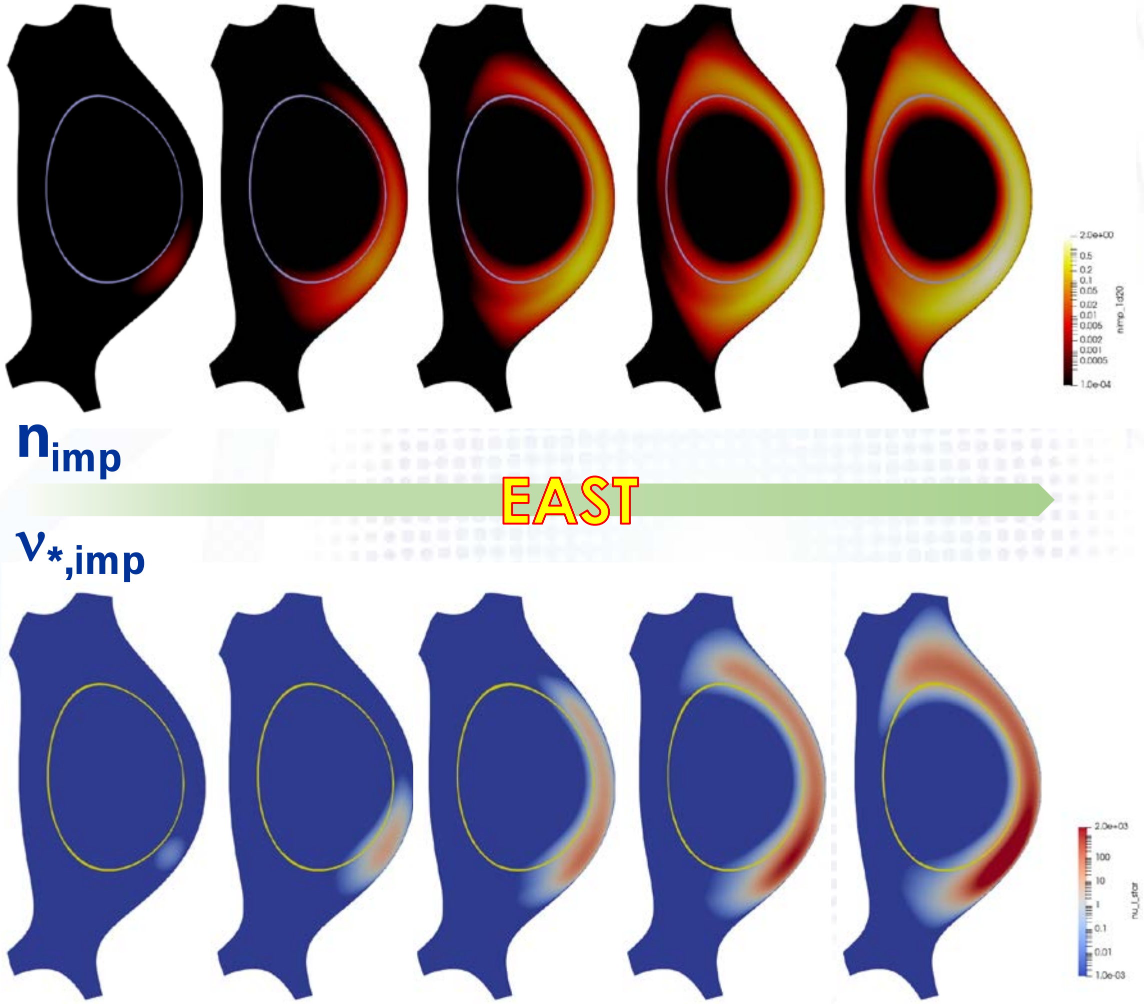

Evolution of plasma parameters presents clear change in collisionality and amount of impurity

- **Simulation results via JOREK with fixed viscosity show that the collisionality increases quickly from the banana to the P-S regime.**

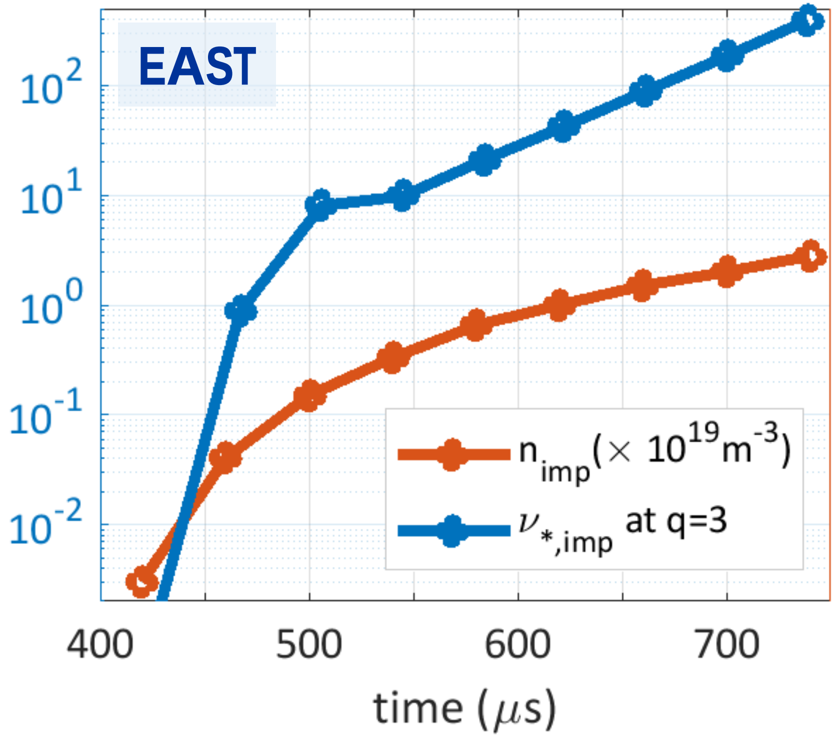

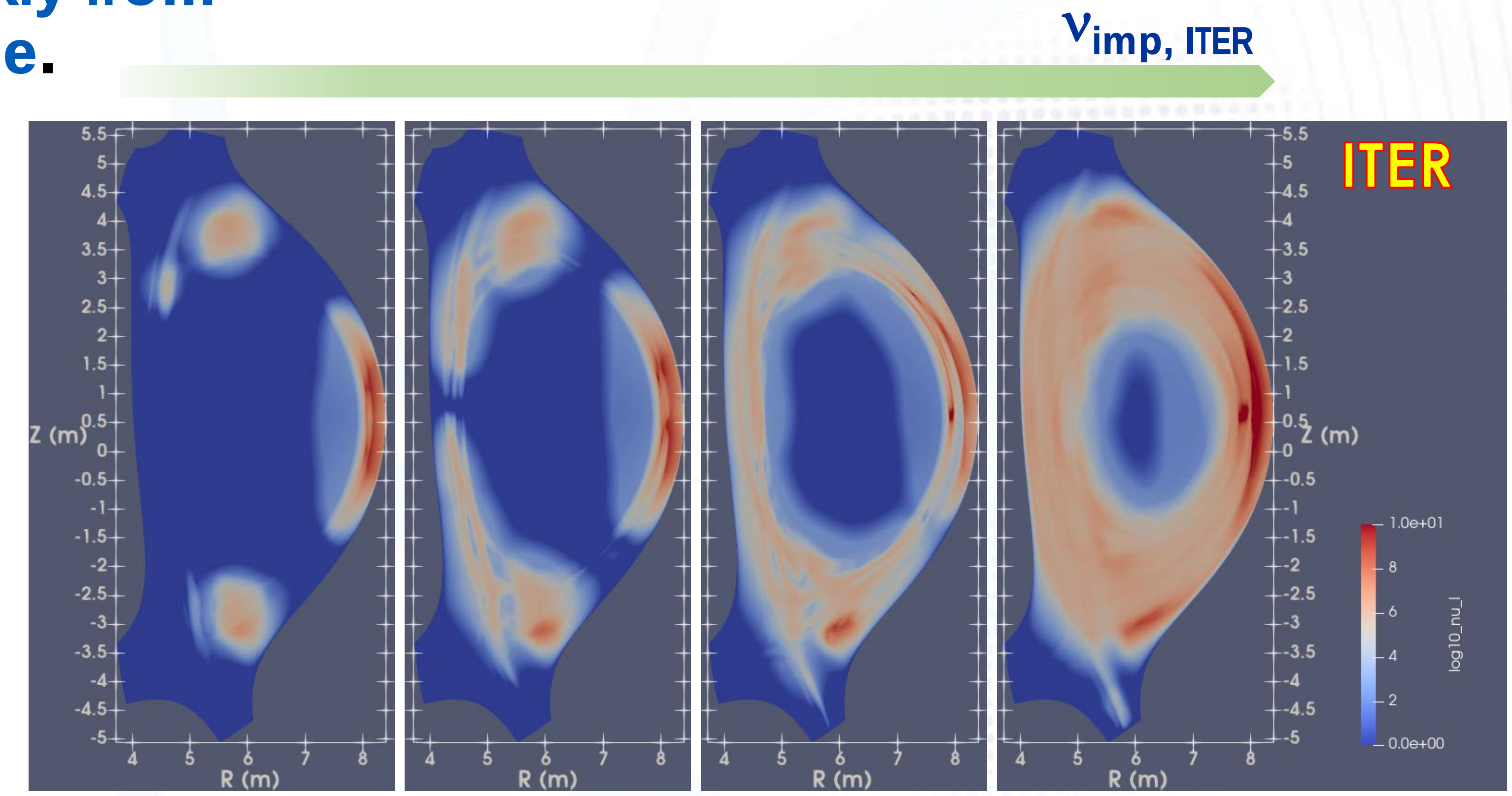

Nuclear Fusion 64 (2024) 086005

Interpretive JOREK simulation of TQ triggered by MGI

Simulation setup for disruptions by JOREK

- **Models: single-fluid reduced nonlinear MHD model with non-equilibrium impurity treatment.**
  - *The perpendicular diffusivity are chosen to keep the profile approximately constant in the simulation.*

- **Simulation setup: A typical L-mode plasma with I_P ~ 0.4 MA and q_{min} ~ 1.6.**
  - *The initial core T_e is ~2.2 keV, electron and ion temperatures are assumed to be equal, and the core n_e is ~3.6×10^{19} m^{-3}.*
  - *MGI triggered.*

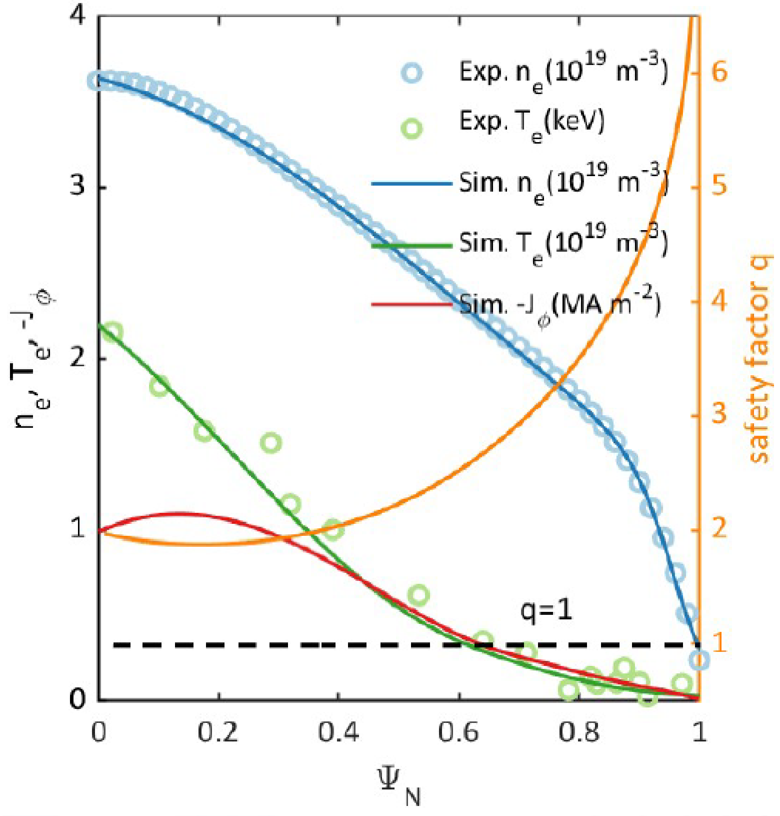

Nucl. Fusion 64 (2024) 112016

Impurity trajectory in toroidal direction

- **Motion asymmetrically in toroidal direction**
  - *It is driven by a parallel electric field $E_{//}$ of approximately 30 V/m.*

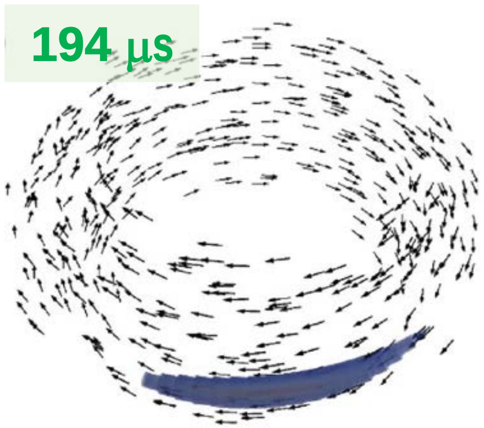

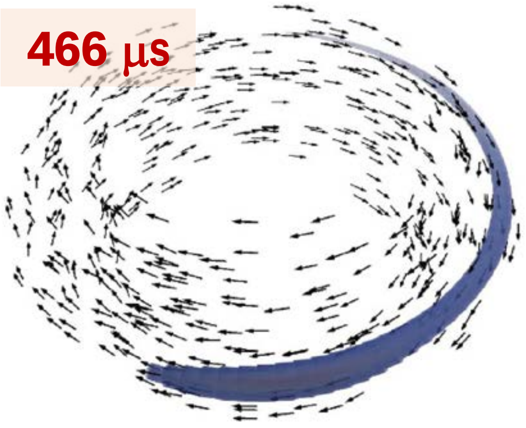

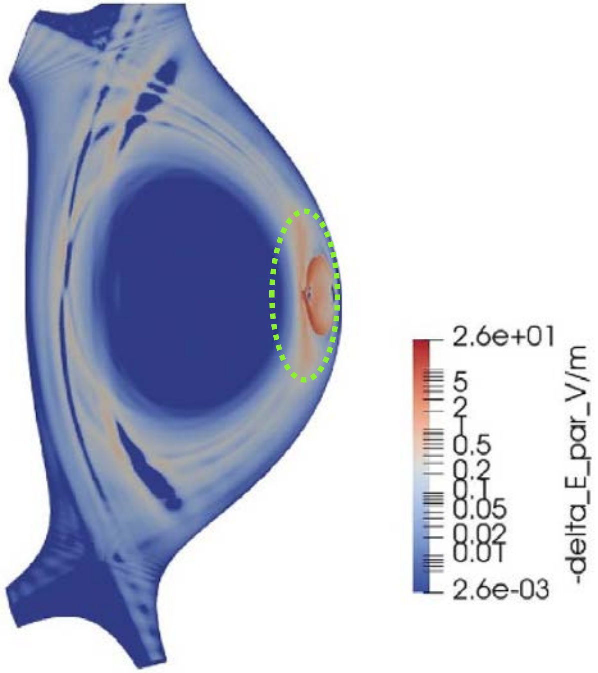

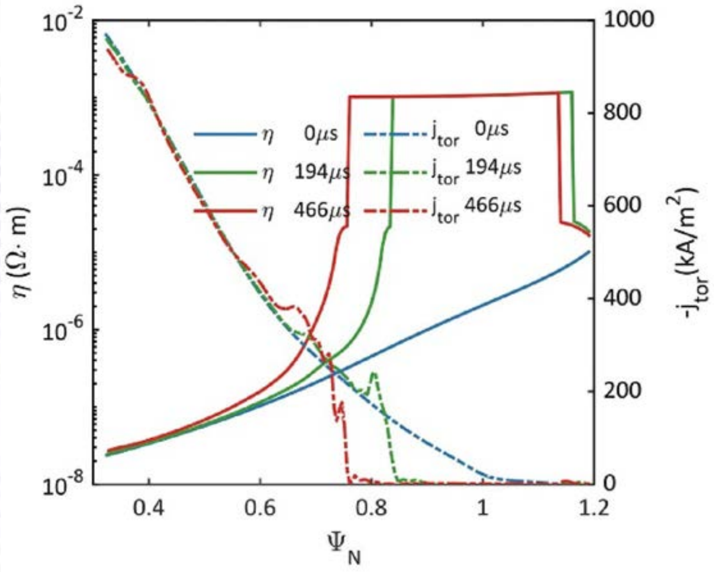

Current relaxation time > Resistivity increase time

Te evolution during typical double-stage TQ

- Two distinct temperature collapses occur at t_1 = 850 μs and t_2 = 1400 μs.
  - *First collapse: The edge temperature collapses firstly, companied with core thermal energy loss and the formation of a temperature plateau.*

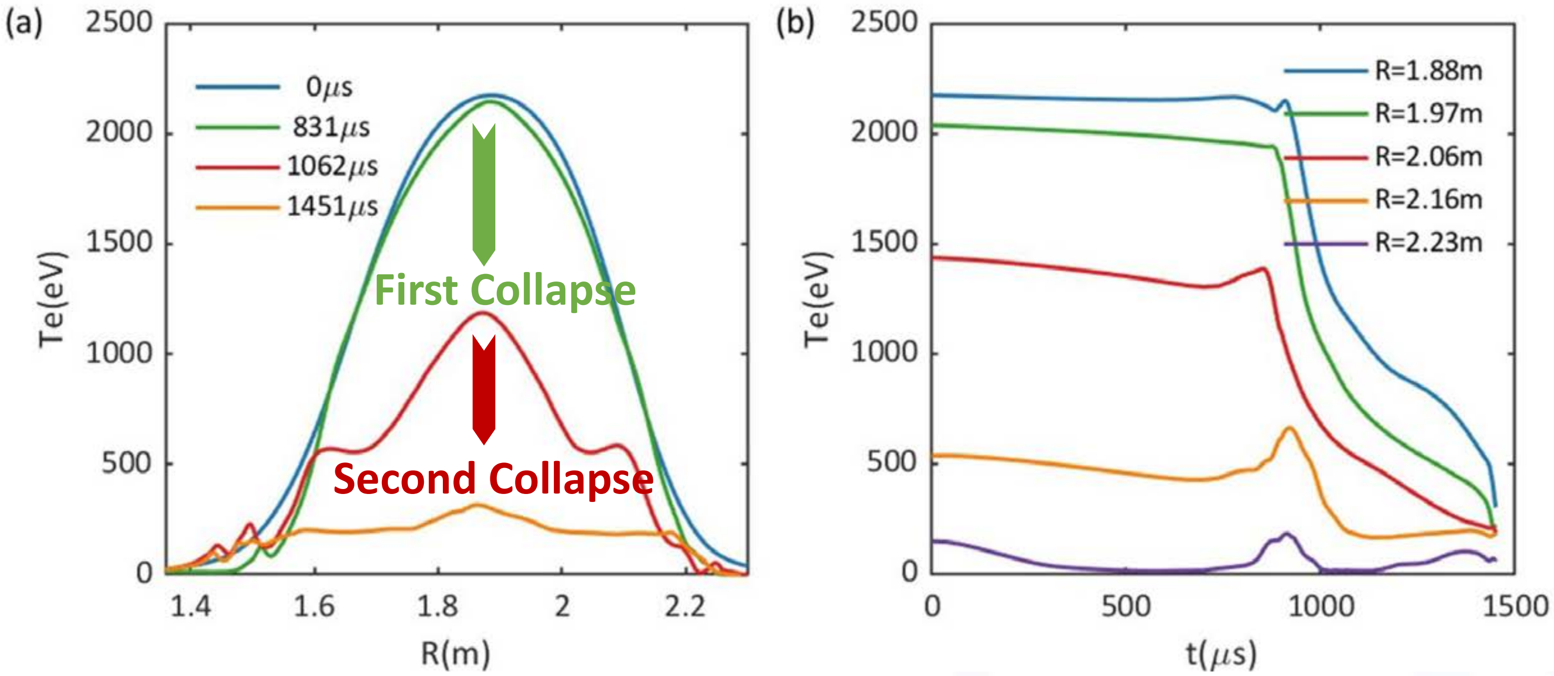

Nucl. Fusion 65 (2025) 056028

Te evolution during typical double-stage TQ

- **Two distinct temperature collapses occur at t_1 = 850 μs and t_2 = 1400 μs.**
  - ***First collapse*: *The edge temperature collapses firstly, companied with core thermal energy loss and the formation of a temperature plateau.***
  - ***consistent with the experimental observation.***

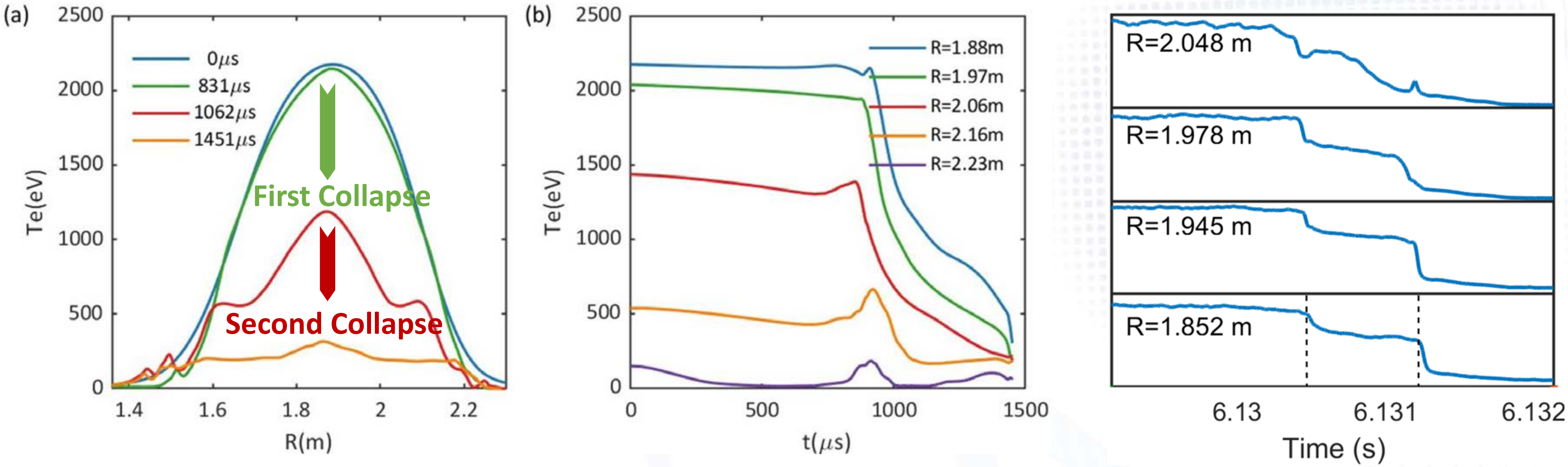

Nucl. Fusion 65 (2025) 056028

MHD activities during typical double-stage TQ

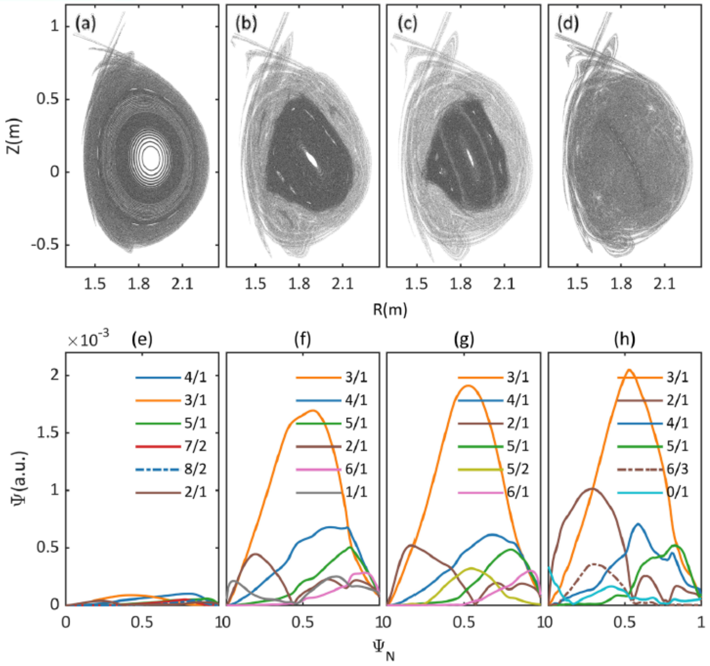

- **1-2 Delay stage**
  - ***The growth of the 2/1 island results in a decrease in core temperature. The 3/1 mode couples with the 4/1 and 5/1 modes, contributing to edge stochasticity.***
- **Second collapse**
  - ***Non-linear interaction between the 3/1 and 2/1 modes primarily leads to global stochasticity.***

MHD activities during typical double-stage TQ

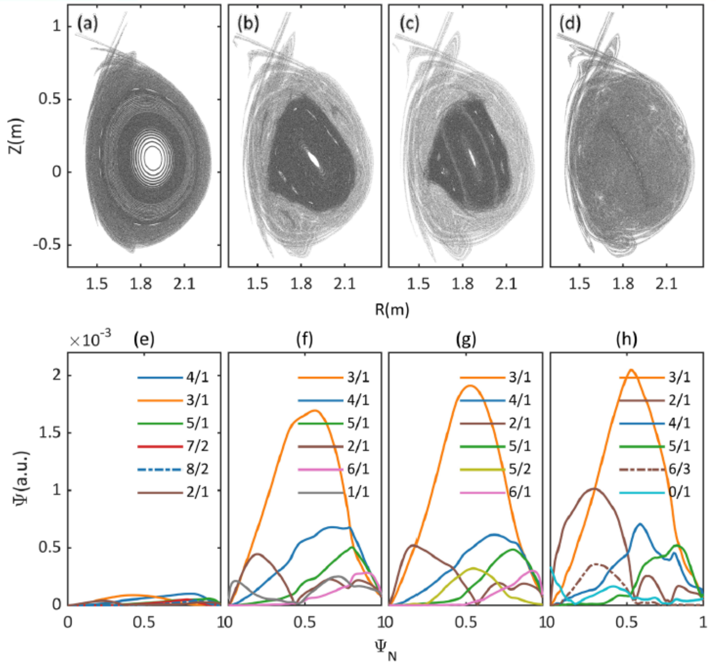

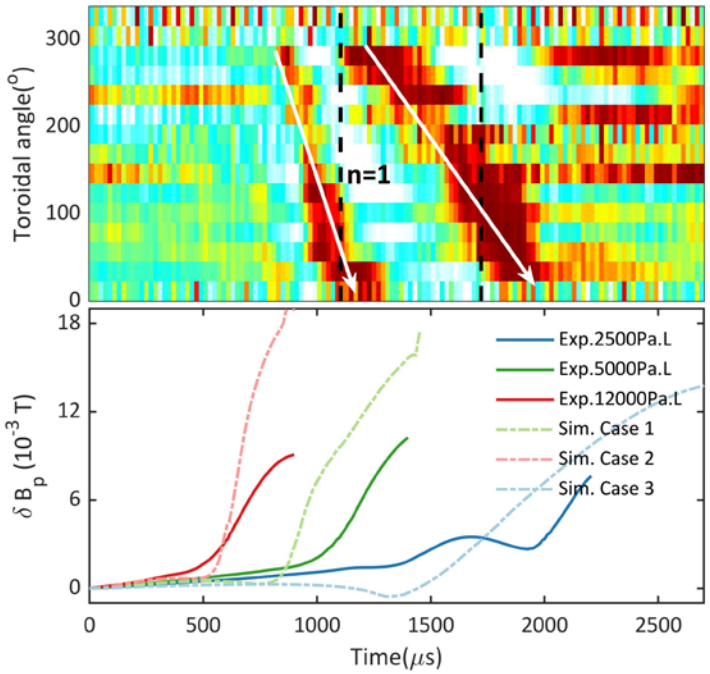

The n=1 mode grows significantly before the TQ, consistent with the simulation results.

- **1-2 Delay stage**
  - *The growth of the 2/1 island results in a decrease in core temperature. The 3/1 mode couples with the 4/1 and 5/1 modes, contributing to edge stochasticity.*
- **Second collapse**
  - *Non-linear interaction between the 3/1 and 2/1 modes primarily leads to global stochasticity.*

Strike point splitting on the divertor during the TQ

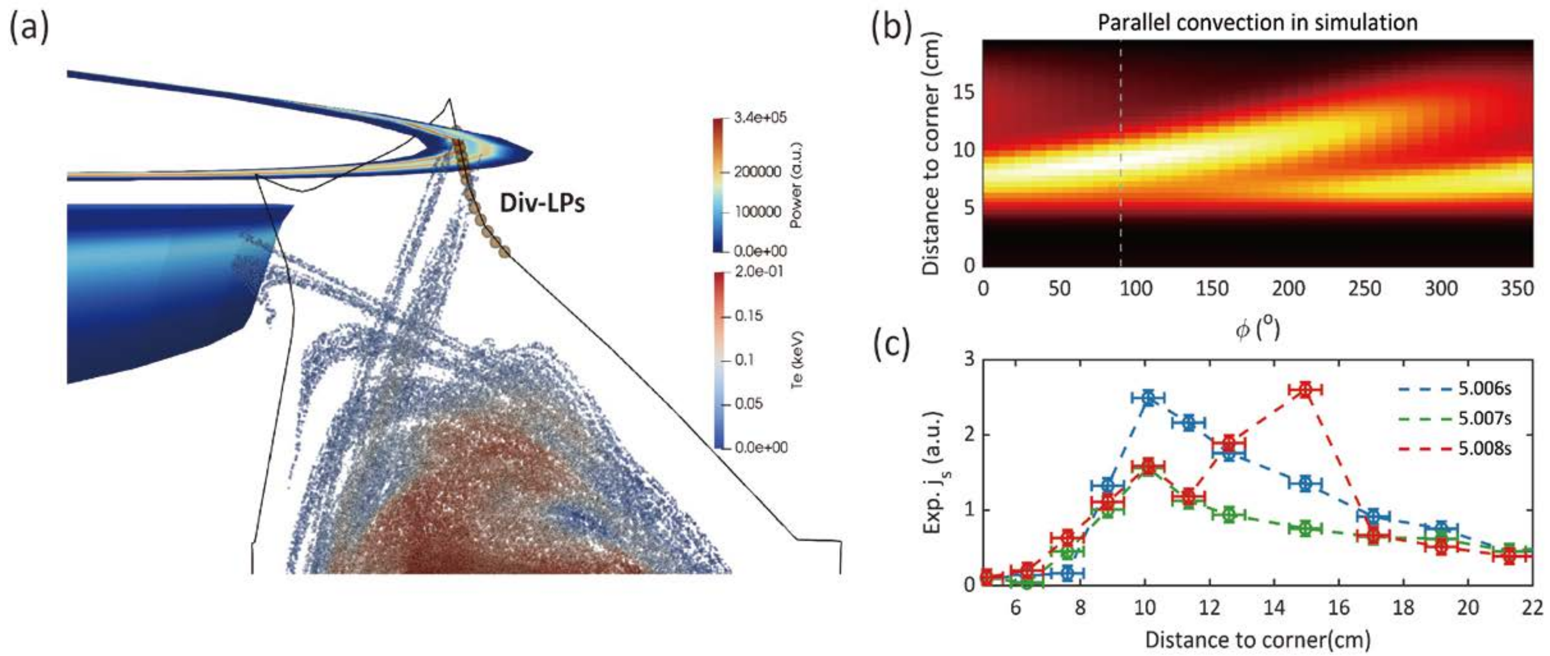

Saturated ion flux measurement obtained by Langmuir probes consistent with simulation results

- **The simulated parallel convective particle flux at the upper-outer target, combined with the strike-point splitting, exhibits an n = 1 structure.**
  - ***This result provides an explanation for the broadening of energy deposition width during the TQ in ASDEX Upgrade and JET.***

Plasma Phys. Control. Fusion 46 (2004) 971
J. Nucl. Mater. 363–365 (2007) 1006–1010

Summary

- **Thermal quench dynamics in massive-impurity-injection triggered EAST disruptions have been demonstrated in experiments and simulations.**
  - ✓ **Sudden change in mode frequency**: ***A sudden change of the radial electric field (E_r), caused by collisionality transition from the banana to the P–S regime, can drive the poloidal rotation and enhance impurity influx.***
  - ✓ **Double-stage TQ**: ***The 3/1 mode couples with the 4/1 and 5/1 modes, contributing to edge stochasticity. The non-linear interaction between the 3/1 and 2/1 modes primarily leads to global stochastic.***
  - ✓ **3D splitting of heat flux**: ***The parallel convective particle flux at the upper-outer target, combined with the strike-point splitting, exhibits an n = 1 structure.***

Summary

- **Thermal quench dynamics in massive-impurity-injection triggered EAST disruptions have been demonstrated in experiments and simulations.**
  - ✓ **Sudden change in mode frequency**: ***A sudden change of the radial electric field (E_r), caused by collisionality transition from the banana to the P–S regime, can drive the poloidal rotation and enhance impurity influx.***
  - ✓ **Double-stage TQ**: ***The 3/1 mode couples with the 4/1 and 5/1 modes, contributing to edge stochasticity. The non-linear interaction between the 3/1 and 2/1 modes primarily leads to global stochastic.***
  - ✓ **3D splitting of heat flux**: ***The parallel convective particle flux at the upper-outer target, combined with the strike-point splitting, exhibits an n = 1 structure.***

Thanks!

Backup

Parameter dependence of mode frequency

- **The phenomenon has been observed by species and numbers of impurities, and heating methods.**
  - ***Amount scan: Earlier and faster reversion of rotation direction***
  - ***The mode frequency changes from -5 kHz to −9 kHz in ~ 0.5 ms after argon injection into RF-heating plasmas.***
  - ***The mode frequency after argon injection seems lower than after neon injection.***

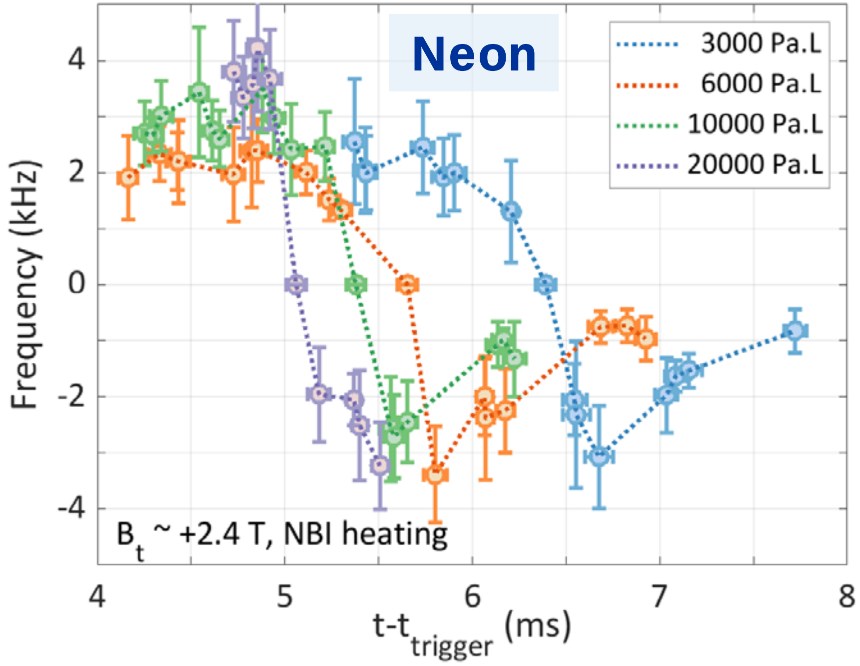

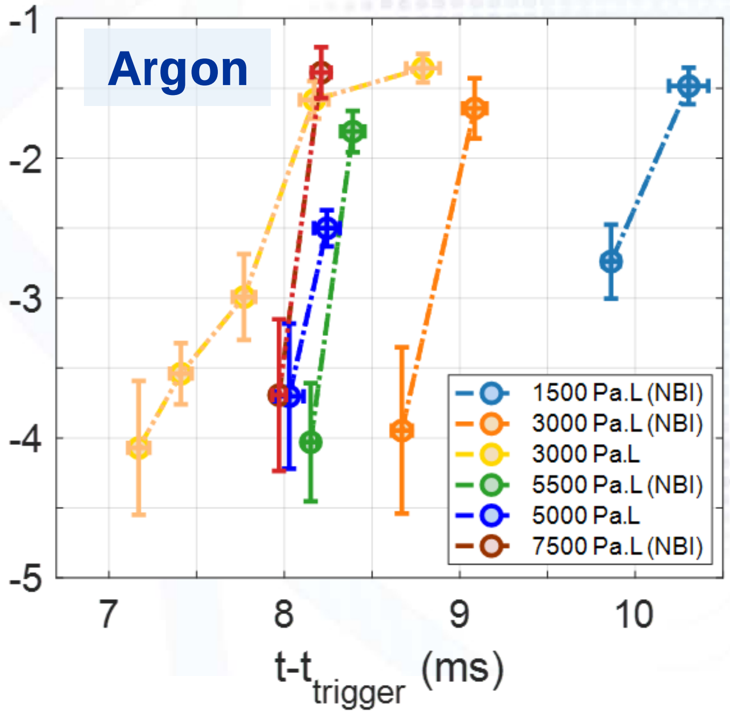

Models and simulation settings

Models: **single-fluid reduced MHD model** with **non-equilibrium impurity treatment**

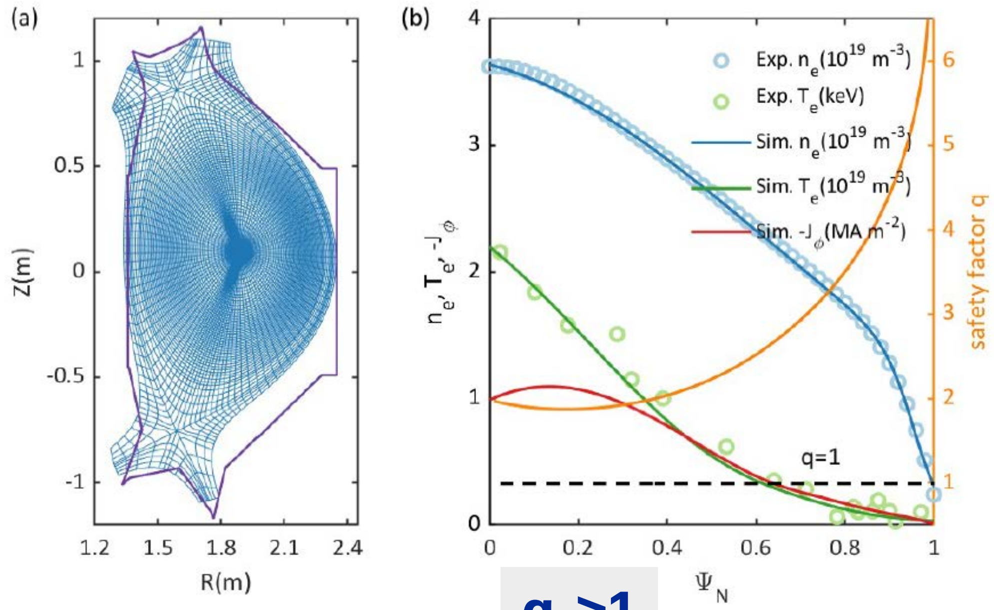

q_0>1

initial central resistivity	η_0	$8\times10^{-9}\ \Omega\cdot m$
dynamic viscosity	μ_0	$3\times10^{-6}\ kg\cdot m^{-1}s^{-1}$
	$\mu_{\|\|,0}$	$1.5\times10^{-5}\ kg\cdot m^{-1}s^{-1}$
particle diffusivities	$D_{\perp,0}$	$1\ m^2s^{-1}$
	$D_{\|\|,0}$	$1.3\times10^{5}\ m^2s^{-1}$
heat diffusivity	$\chi_{\perp,0}$	$15\ m^2s^{-1}$
	$\chi_{\|\|,0}$	$7.7\times10^{10}\ m^2s^{-1}$

The perpendicular diffusivity are chosen to keep the profile approximately constant in the simulation.

Impurity trajectories

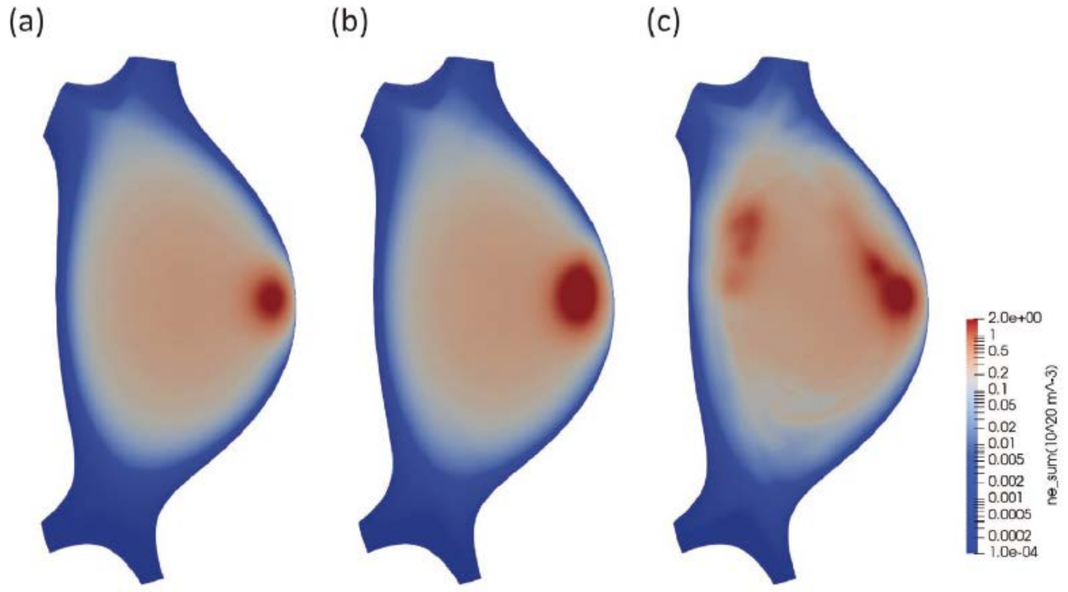

Neon particles

Move inward along the major radius

Deposit at Ψ_N~0.7

Extend along magnetic field lines

Create new deposition spots at different poloidal positions